Micrometer-Wide NbN Strips for Photon-Number-Resolving Detection

M. Dryazgov,[1,2] Yu. Korneeva,[2] and A. Korneev[1,2,*]

[1] *HSE University, Moscow 101000, Russia*

[2] *Institute of Nanotechnology of Microelectronics of the Russian Academy of Sciences, Moscow 115487, Russia*

We report the development of photon-number-resolving superconducting single-photon detector with micron-scale NbN strips. The detector is designed as serial meander-shaped strips with resistors connected in parallel to each strip. We investigate the performance of the detectors comprising of 5–14 strips with the widths in the range 0.3–1 µm and covering an area as large as 70×70 µm^2 making it feasible for coupling to multimode fibers. We demonstrate resolution of up to six photons and analyze the sources of errors in photon-number resolution.

I. INTRODUCTION

Superconducting single-photon detectors (SSPDs) have been known for two decades [1]. The operation of a SSPD is based on local breaking of superconductivity in a strip carrying sufficiently high current [2]. With the high speed and efficiency at telecommunication wavelengths, they have found applications in many areas [3]. The development of quantum technologies requires not only the knowledge about the presence of a photon, but also information about the number of photons in the optical pulse, i.e., quantum cryptography and quantum computing benefit from photon-number-resolving detectors (PNR). Single-photon avalanche diodes (SPAD) and photomultiplier tubes (PMTs) although widely used in quantum optics, are not PNR capable.

Tungsten transition-edge sensors (TES) are known to be capable to resolve the total amount of absorbed energy and thus to determine either a photon wavelength or a number of photons of a given wavelength. Although they demonstrate detection efficiency of 95% in near infrared [4], these detectors are operated at 100-mK temperature, have a long thermal recovery time (800 ns), very low repetition rate (50 kHz), which make them not attractive for state-of-the-art applications in quantum optics.

On the other hand, with the recently reported detection efficiency of 98% [5], SSPD is feasible for PNR implementation. Two major PNR configurations of SSPD have been reported earlier [6]. Both of them implement spatial division of incoming photon flux and feeding it to individual SSPD meanders. The difference of these approaches is in the way how meanders are connected to produce a voltage pulse with the amplitude depending on the number

of simultaneously registered photons: (1) SSPD meanders are connected in parallel with the resistors connected in series to the meanders [7], and (2) serial connection of meanders and each meander has a resistor in parallel [8]. A waveguide-integrated version of PNR SSPD has also been reported [9]: detection of up to four photons is demonstrated with 24% single-photon detection efficiency, which is still low for many practical applications. Whereas for traditional fiber-coupled PNR SSPD up to 86% detection efficiency is reported [10].

Another approach for PNR with SSPD is to use the impedance transformer tapered microstrip or co-planar line to match kΩ impedance of the hotspot with 50Ω of the transmission line. In this way one can distinguish the number of hotspots created by absorbed photons by either the rise time [11], the amplitude of the pulse [12], or by the time delay between voltage pulses read from both ends of the line [13]. In some case when cryogenic amplifiers are used the PNR capability can be achieved even with traditional SSPDs by using an advanced technique of waveform analysis [14]. Although this approach is interesting and fruitful, it seems that it can provide only a few-photon resolution (up to 6) while the serial connection approach demonstrated previously up to 24 photons [15].

One of the main issues in the design of PNR SSPD is the capability to produce a distinguishable voltage responses for photon states, which differ by only one photon, e.g., to distinguish reliably between 1 and 2, or 2 and 3, etc. photons. Increasing the number of meanders in PNR SSPD (and the number of resolvable photons) results in the reduction of voltage difference of the response for the neighboring photon states and is ultimately limited by the electrical noise background. On the other hand, the voltage can be increased by increasing the bias currents of the meanders, which can be straightforwardly achieved by

*aakorneev@hse.ru

using materials with high critical-current densities, such as Nb-Ti-N or NbN, and making meander strip micronwide [16].

The use of microwide superconducting strips makes it possible to fabricate detectors with a larger area with a nonincreasing kinetic inductance, and expand the scope of its application: for example, enabling efficient coupling to multimode fibers.

We report here our analysis of the photon-number-resolution accuracy by the PNR SSPD made of submicron-wide NbN strips. For our study we fabricate and characterize PNR SSPDs with serial connected strips. Although detection efficiency of our devices is still limited by the absorption of thin film and is far from desirable 100%, we demonstrate the multiphoton response as a proof-of-principle and the capability of the detectors to correctly distinguish up to seven photons. We also use these results to extrapolate the ultimate performance of the device and compare it with the case of parallel connection of strips.

II. DEVICE DESIGN AND EXPERIMENTAL METHODS

Figure 1(a) shows an example of the seven-section serial PNR SSPD with 1-μm-wide strip (sample 2877 no. 9). The equivalent circuit diagram is shown in Fig. 1(b): $L_1 \cdots L_k$ represent the kinetic inductances of the superconducting strips, resistors $R_{n1} \cdots R_{nk}$ represent the normal domains after photon absorption, R_p are additional resistors fabricated on-chip and required for proper impedance matching of normal domains with the transmission line and simultaneously prevent "latching," Z_0 is the impedance of the transmission line (coaxial cable). We use an electrothermal model to calculate the optimal values of R_p [17].

For the fabrication of the PNR detector, an NbN layer is deposited by dc magnetron sputtering [18,19]. The sheet resistance at room temperature R_s of the fabricated films is in range 550–700Ω. According to our recent study [18], for the saturated detection efficiency in micronwide NbN strips one should use films with larger sheet resistances, preferably higher than 630Ω. Simultaneously, higher R_s leads to smaller critical current and lower photon absorption, both are not favorable for optimal performance of PNR. While low absorption of the film can be compensated by a proper integration of the detector in an optical cavity, here we use a simple cavity comprised of Au mirror (80-nm-thick) and 160-nm-thick Si_3N_4 layer fabricated on a dielectric substrate of 430-μm-thick Al_2O_3 as shown in Fig. 1(c).

A meander is patterned using electron-beam lithography in a positive-tone resist. To prevent the current-crowding effect in the turns of the meander, these turns are designed using the formulas from Clem and Berggren [20], and allowed us to increase the filling factor up to 0.67. Then resistors are fabricated from Ti film with sheet resistance of
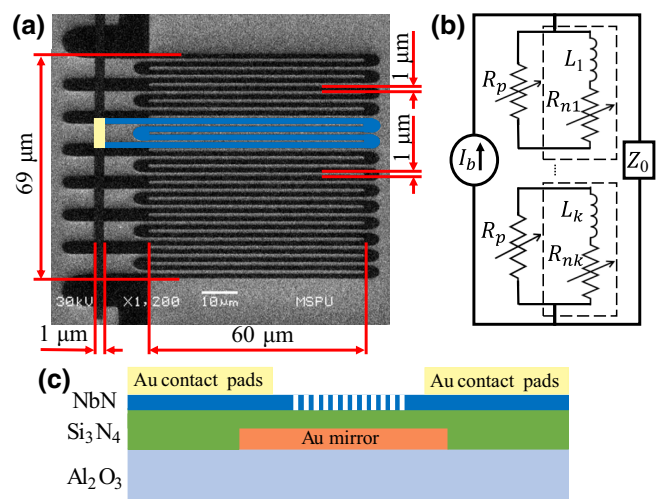

FIG. 1. (a) SEM image of serial PNR SSPD, one section and the corresponding resistor are highlighted in color. (b) Circuit diagram of serial PNR SSPD. (c) Schematic structure of the optical cavity.

15Ω at room temperature. In the presented example, every third turn of the meander is extended and connected with the Ti resistor (marked by yellow color), thereby creating one section of PNR. For simplicity of the fabrication, all the resistors are patterned as a single rectangle covering all the extensions of the corresponding NbN sections of the PNR detector.

The properties of the studied PNR detectors are summarized in Table I. The samples passed initial screening at 4.2-K temperature: critical currents and capability to produce voltage pulses of different amplitudes depending on the number of photons per optical pulse are tested. Then the best devices are characterized at 1.7 K as well. The *I-V* curves are measured with the home-built dc source, which can operate in both constant-current and constant-voltage modes. An additional resistor of 20Ω is connected in series in the dc port of bias *T* to suppress instabilities of the dc source and radio noise induced on the dc cables.

For optical characterization, we use an attenuated fiber-coupled pulsed laser with the wavelength 1064 nm and operated at 200-MHz repetition rate. Although many applications rely on a telecom wavelength of 1550 nm, shorter wavelengths are interesting when $(In, Ga)As$ quantum dots are used as single-photon sources operating around 925-nm wavelength. Thus, our choice of the wavelength is more relevant for such applications.

The waveforms from the PNR detector are amplified by two rf amplifiers Mini-Circuits ZFL-1000LN (0.1–1000-MHz band, 20-dB gain, and 2.9-dB noise figure) and captured with the digital oscilloscope. Photon count rate is measured with Agilent 53131A universal counter. Discrimination of pulses with different amplitudes is performed by setting a different trigger threshold on the

TABLE I.   Properties of the PNR detectors studied here.

Sample	Sensitive area (μm)	Number of sections	Strip width (μm)	Filling factor	R_s (Ω)	T_c (K)	I_c (1.7K) (μA)	I_c/I_{dep}
2647-1 no. 6	54 × 22	5	0.596	0.5	585	8.9	68	0.48
2647-1 no. 13	21 × 18	7	0.34	0.5	585	8.9	43	0.54
2647-1 no. 20	35 × 30	7	0.57	0.5	585	8.9	79	0.58
2647-2 no. 6	63 × 58	14	0.50	0.5	585	8.9	63	0.53
2647-2 no. 17	53 × 44	5	1.0	0.5	585	8.9	110	0.47
2647-2 no. 20	69 × 60	7	1.0	0.5	585	8.9	112	0.47
2659 no. 16	35 × 30	7	0.51	0.5	660	7.6	45	0.60
2659 no. 18	51 × 46	11	0.51	0.5	660	7.6	45	0.60
2877 no. 9	54 × 40	7	1.0	0.67	660	8.0	104	0.62

counter and then subtracting count rates at higher thresholds from count rates at lower thresholds (as the pulses of all amplitudes above the threshold are counted).

III. EXPERIMENTAL RESULTS

A. Critical current

The *I-V* curve shown in Fig. 2 is measured for the seven-section device 2647-2 no. 20 but is typical for many studied samples. One may note that the main peak at the critical current is followed by a number of small peaks as shown in the enlarged part in Fig. 2. We attribute these peaks to the subsequent switching to normal state of different sections of the detector, which have slightly different critical currents due to film inhomogeneity or defects of strip patterning. The increase of the resistance after each peak is in the range 23–27Ω, which corresponds to the resistors fabricated parallel to each section (the values in the plot indicate the resistances on the linear parts of the
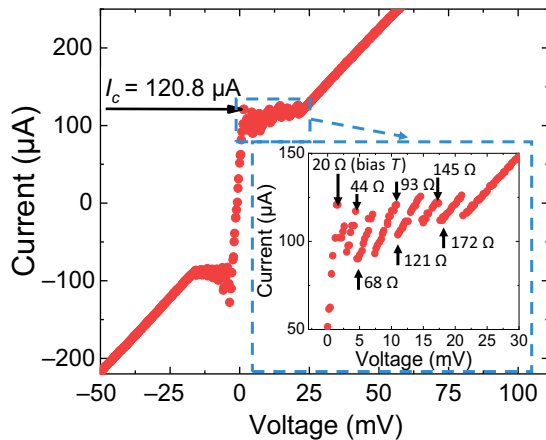
I-V curve, the slope of the initial superconducting part is due to 20Ω serial resistor in bias *T*).

The observed effect can be used as a tool to judge about the quality of our devices. For the device presented in Fig. 2 critical currents of the sections vary in range 109–127 μA (with the standard deviation of 5.8 μA).

We also calculate depairing currents for the studied devices at the operation temperature of 1.7 K using formula by Clem and Kogan [21]:

$$j_{dep}(T) = 0.74 \frac{[\Delta(0)]^{3/2}}{eR_s\sqrt{\hbar D}} \left[1 - \left(\frac{T}{T_c}\right)^2\right]^{3/2}, \quad (1)$$

where superconducting gap at 0 K is calculated as $\Delta(0) = 1.76k_BT_c$, e is electron charge, R_s is the sheet resistance, for diffusivity D we take 0.4 cm^2/s which is typical for NbN. Most of our devices feature ratio I_c/I_{dep} near 0.6 or above, which is in the agreement with theoretical requirement for single-photon detection in micron-wide strips [22] and our previous experimental study [16].

B. Detection efficiency

We measure detection efficiency η at 1064-nm wavelength in single-photon regime at 1.7-K temperature. The result is presented in Fig. 3 where we plot detection efficiencies versus normalized bias currents I_b/I_c. We observe saturation only for 0.5-μm-wide devices made from film with $R_s = 660\Omega$ (2659 no. 16), whereas for devices with $R_s = 585\Omega$ (2647-1 no. 6, 2647-1 no. 13, 2647-2 no. 20) the saturation plateau is hardly observed even for 0.3-μm-wide detectors. For 0.5–1-μm-wide devices we do not observe any saturation plateau at all. We attribute this fact to insufficiently thin film, or rather small R_s. This fact is in a good agreement with our previous inquires made on straight NbN strips and meanders: for 1-μm-wide strips a saturation of η at wavelength above 1 μm is observed when $R_s > 630\Omega$ [18].

The maximum η of about 30% observed in the plot in Fig. 3 is actually limited by the absorption of our devices, which are integrated in a rather simple optical cavity.
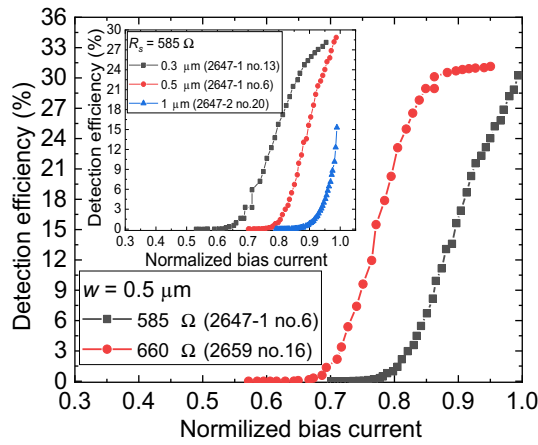

FIG. 2.   *I-V* curve of a seven-section PNR SSPD (2647-2 no. 20). Critical current $I_c = 120.8$ μA. Parallel resistances $R_p \approx 23\Omega$ are determined from the slopes of the peaks of the *I-V* curve (values in the inset indicate the resistance of the corresponding straight parts of the curve).

FIG. 3. Detection efficiency (at 1064 nm) for PNR SSPDs with strip widths 0.5 µm for R_s equal to 585 and 660Ω. The saturation is observed only for $R_s = 660$Ω. Inset: detection efficiency at 1064-nm wavelength versus normalized bias currents I_b/I_c measured for PNR SSPDs with strip widths 0.3, 0.5, and 1 µm and $R_s = 585$Ω. Saturation is not observed even for strip width 0.3 µm.

We believe that the usage of more sophisticated cavities such as Bragg reflectors together with an antireflection coating on top of the detector may provide detection efficiency above 90% at the target wavelength (see more in Appendix B).

C. PNR capability

Figure 4(a) shows the oscilloscope traces of voltage pulses measured for sample 2877 no. 9 corresponding to simultaneous triggering of one to seven sections. The distribution histogram (in the inset) demonstrates good discrimination between voltage pulses of different amplitudes. To prove truly photon-number-resolving capability we measure photon-count statistics at various attenuation levels of the laser. The multiphoton counts are measured by adjusting counter trigger to the voltage levels corresponding to one-, two-, three-, etc. photons and subtracting from the lower-level counts, the upper-level counts (e.g., to get two-photon counts we subtract counts measured at three-photon trigger level form the counts measured at two-photon trigger level). The photon-count events for different photon numbers as a function of power measured at the fiber input are plotted in Fig. 4(b). According to Poisson distribution, for mean number of photons per pulse $\mu << 1$ single-photon counts are proportional to μ, two-photon counts are proportional to μ^2, three-photon counts are proportional to μ^3, etc, as shown in Fig. 4(b).

Then we compare the resulting distribution with the Poisson distribution for a given mean number of photons μ in a laser pulse. Single-photon counts are proportional to detection efficiency η, two-photon counts are proportional to η^2, m-photon counts are proportional to η^m. Due

to low η, m-photon detection efficiency drops rapidly with increase of m. For clear comparison, we divide experimental count rate for m-photon detection by η^m. The result is shown in Figs. 4(c)–4(h). Blue bars are the experimental photon count. Green bars are the recovered incident number of photons (count rate divided by η^m). Red bars are Poisson distribution. There is a good agreement between green and red bars.

IV. DISCUSSION

For practical applications of PNR it is useful to distinguish between photon states that differ by only one photon, e.g., distinguish between two and three photons. The error in photon-number measurement may arise from two sources: (1) trivial hitting of a single section of the detector by two or more photons, and (2) thermal noise that distorts the waveform transients making wrong voltage discrimination.

The first issue can be resolved by making a considerably large number of sections compared to the number of photons one wishes to resolve. Quantitatively, for a detector comprising of N sections the probability that one photon hits a certain section is $1/N$, the probability that two photons hit the same section is $1/N^2$. Then, the probability that two photons hit two different sections is given by $(N-1)/N$ (when the first photon hits a sections, there are $N-1$ other sections available for the second photon). Similarly, the probability that three photons hit three different sections is given as a product of probabilities:

$$P(3) = \frac{N-1}{N} \times \frac{N-2}{N} = \frac{(N-1)(N-2)}{N^2}.$$

These results are illustrated in Fig. 5. This simple math predicts that two photons can be resolved with the probability higher than 0.95 if there are 20 or more sections of the detector. To distinguish three photons with the probability higher 0.95 one needs 60 or more sections.

This result has an implication for the result presented in Fig. 4(a): the probability, e.g., that six-photon pulse actually corresponds to six photons is very small, due to indistinguishable absorption of several photons in the same section. To achieve a reasonable accuracy one has to make much more sections than the desired number of photons to be resolved. Even the resolution of three photons with rather moderate accuracy of 85% requires 20 section.

Moreover, these considerations are valid only in the assumption of near unity detection efficiency of the section which is also an issue: although 98% detection efficiency was demonstrated in the lab [5], for commercial SSPDs a routinely claimed detection efficiency is about 85%.

On the other hand, increasing the number of sections leads to the reduction in pulse-amplitude difference for a different number of photons. To estimate the ultimate number of available sections for a given noise level we
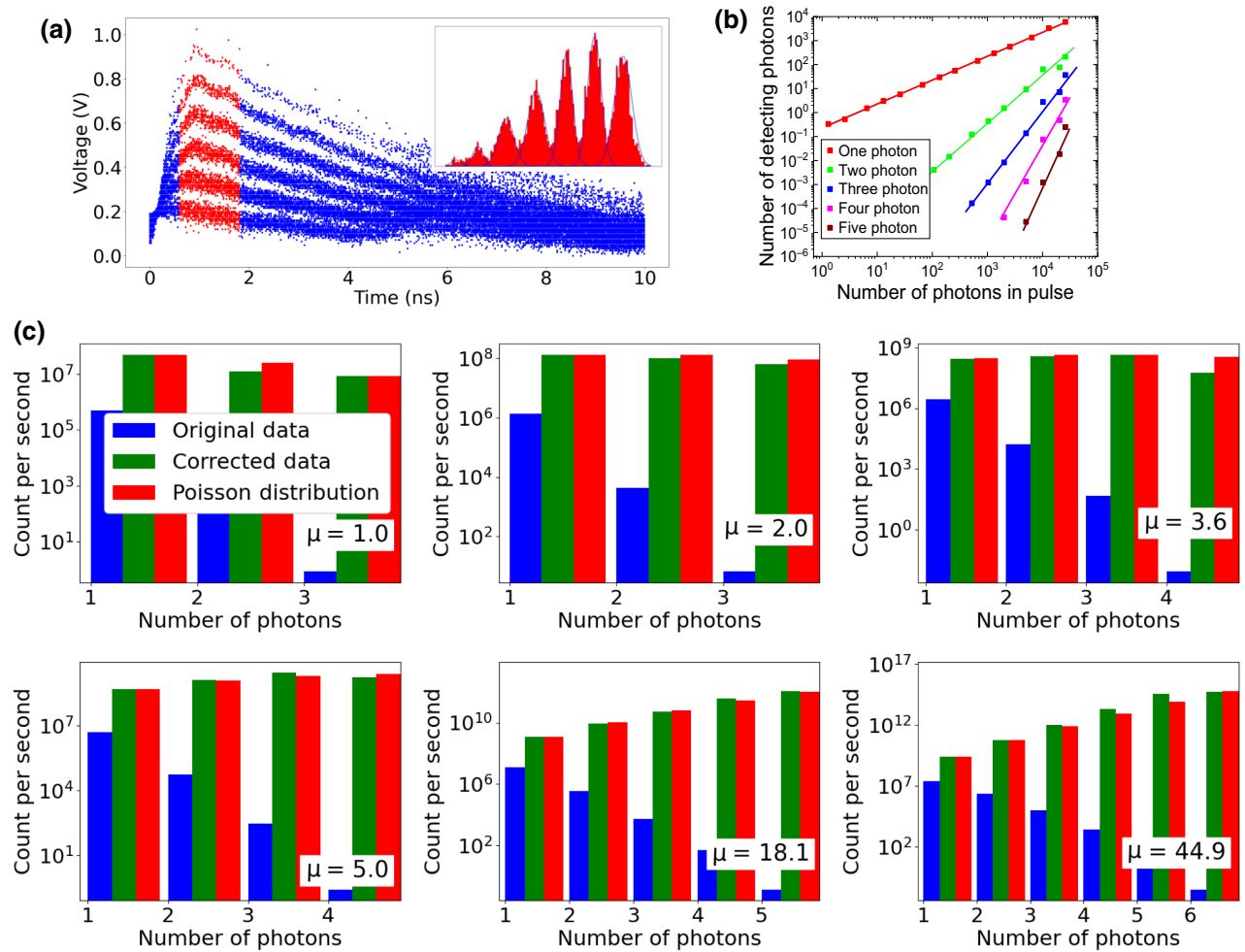
FIG. 4. (a) Waveform transients of voltage pulses representing one to seven photon absorption at $I_b = 93$ μA ($I/I_c = 0.9$). The maximum pulse amplitude is about 1.1 V. The inset presents voltage distribution diagram taken from the waveforms area marked by the red color, seven pulses are perfectly distinguishable. (b) Dependence of one-photon, two-photon, three-photon, four-photon, and five-photon counts per second on the incident photon flux (per second). (c) Poisson distributions with different mean photon number per pulse μ. Blue bars are measured photon counts, green are recovered photon fluxes taking into account detection efficiency of the detector, red are Poisson distribution.

set a simple criterion that the minimum difference of the amplitudes corresponding to the "adjacent" photon numbers (i.e., photon numbers, which differ by 1, e.g., 4 and 5, 5 and 6, etc.) should be at least 1.5 of noise rms voltage. A more detailed effect of noise on the number of resolvable photons is considered in Ref. [23].

To estimate the output voltage of the PNR with a different number of sections we use the results of our simulation with the electrothermal model with optimal choice of the parallel resistors. For the case of room-temperature electronics we choose noise temperature $T_N = 550$ K (this is the case of MiniCirciut ZFL-1000 that we use, noise figure 2.9 dB), and compare it with the performance of cryogenic HEMT amplifier with $T_N = 4$ K (which is the case, e.g., with Cosmic Microwave Technologies, CITLF3-20K). Inset of Fig. 5 shows dependence of the maximum number

of sections when room-temperature amplifiers and HEMT amplifiers are used. Both dependencies are linear versus detector strip width, and the usage of cooled HEMT amplifiers gives by a factor of 2 improvement compared to the room-temperature electronics.

In the literature, the influence of electrical noise on the distinguishability of the photoresponses to the number of incoming photons is not studied well. Recently this issue was addressed in Ref. [24] in a relation to TES detectors. In particular, for two-photon signal the authors achieved the probability p_2^2 of a correct response of the detector to be equal to 0.99999999527. We compare for our sample 2877 no. 9 distribution histograms like shown in Fig. 4(a) to determine the area of overlap for single- and two-photon response amplitudes. The ratio of overlapped area to the area of single-photon distribution is 0.0177,
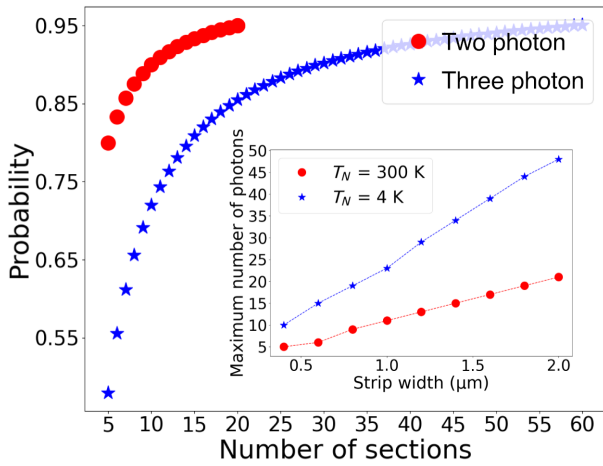
FIG. 5. The probabilities that two photons (red) and three photons (blue) will fall on different sections versus the total number of detector sections (in the assumption of ideal absorption equal to unity). Inset: maximum number of photons that can be resolved with room-temperature amplifiers (red) and with cooled HEMT amplifiers (blue).

thus we conclude that the probability of correct single-photon response is 0.9833 (here we neglect the overlap between single-photon and three-photon distribution). For two-photon events the probability of correct detector output is 0.956. These values are calculated in the assumption of 100% detection efficiency and neglecting several photons hitting the same section. In real life, one should take into account the probability that several photons hit the same section. It reduces probabilities of correct single-photon response to 0.842, and two-photon response to 0.819 (here we neglect probabilities of more than three photons hitting partially the same section).

V. SUMMARY

In conclusion, we demonstrate a PNR detector based on micronwide superconducting strips connected in series. The critical issues for high accuracy in photon-number discrimination with a multisection detector are near-unity detection efficiency and the number of sections of the detector, which should be much larger than the desirable number of resolved photons.

In this paper, with a simple cavity we demonstrate detection efficiency of about 30%. Although we focus on 1064-nm wavelength, similar or even better performance of the detector is expected at telecom wavelength 1550 nm due to higher detection efficiency as shown in Appendix B. Meanwhile, higher detection efficiency can be achieved with the usage of improved cavities, e.g., Bragg reflectors. With such cavities, SSPDs with sub-100-nm-wide strip demonstrate detection efficiency above 98% [5,25]. This fact makes feasible the achievement of near-unity detection efficiency in micronwide strips.

Concerning the number of sections, the resolution of two photons with 95% accuracy requires 20 sections, while for three photons with the same accuracy, almost 60 sections are required. To date, so many sections have not been demonstrated in fiber-coupled implementation yet, while in a waveguide-integrated implementation 100-section detector has been recently reported by Cheng *et al.* [26].

Discrimination of the response amplitudes becomes an issue when the number of sections of the detector increases. From our experimental results and analysis of the thermal noise of the electronics readout, we demonstrate the way to increase signal-to-noise ratio via the increase of the width of the strip. In particular, increase of the strip width to 2 μm enables one-photon resolution with 15-section detector and room-temperature amplifiers and with 50-section detector with HEMT electronics (at 4-K temperature).

With this type of a PNR detector, two types of possible applications seem to be feasible: (1) Statistical measurements with rather a large number of photons (about 10 or a bit more per optical pulse). In this case, original photon statistics can be recovered from the experimental results using the properties of the detector: detection efficiency and the number of sections. Such applications can be characterization of light sources [27], or, e.g., quantum discrimination of laser and thermal light [28]. (2) Applications when the knowledge about the exact number of photons in each measurement is relevant, such as quantum cryptography [29] or quantum computation. In many such applications it is enough to be able to discriminate between one and more than one photon. In this case, the proposed type of detector may be a device of choice providing high count rate, low timing jitter, and negligibly low dark counts. Meanwhile, applications such as boson sampling [30] or multiphoton quantum-state engineering [31] in present implementations resolve about ten photons and may require PNR with about 100 sections.

ACKNOWLEDGMENTS

APPENDIX A: COMPARISON OF SERIAL AND PARALLEL PNRS

An alternative configuration of the PNR detector is a number of superconducting strips connected in parallel, and resistors R_p connected in series to each strip (Fig. 6). When several sections are triggered, the currents are redistributed between other sections and the load Z_0, causing a voltage pulse with the amplitude depending on the number
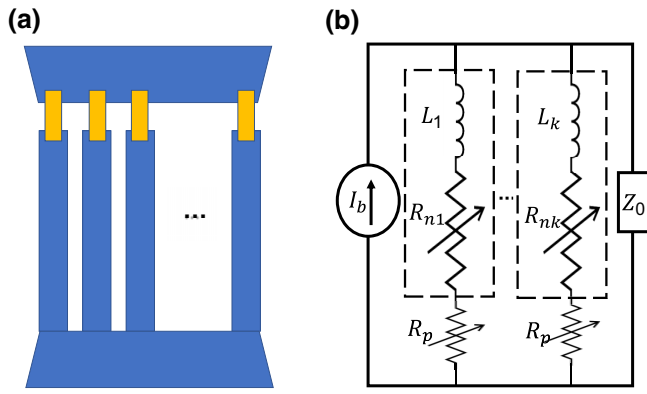
(a)   **(b)**

FIG. 6. Schematic design (a) and equivalent circuit (b) for PNR with the sections connected in parallel. Each section can be made as a straight strip (blue) and should have a resistor connected in series (yellow rectangle), which ensures equal current distribution between sections, and prevents shunting and avalanche switching of the sections.
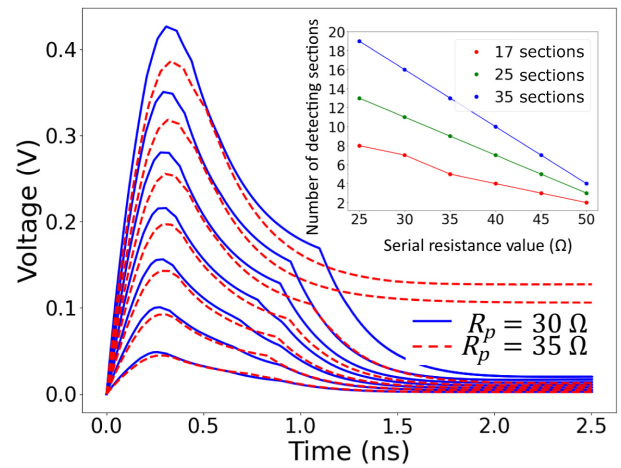

FIG. 7. Simulation of a PNR detector consisting of 17 parallel-connected sections. Blue lines are voltage transients for PNR with $R_p = 30\Omega$, the operation of seven sections is observed. Red dashed lines are voltage transients for PNR with $R_p = 35\Omega$, the operation of five sections maximum is possible, while the simultaneous switch of six and more sections leads to avalanche switch of all the sections followed by latching. Insert: the number of sections available for photon detection depending on the value of R_p for a different total number of sections.

of triggered sections. One of the advantages of this configuration is its capability to realize high filling factor by the usage of straight strips instead of meanders and reducing the gap between the strips. Meanwhile, a "parallel" PNR has a peculiarity of its operation: when a certain number of sections are triggered, the current in the nontriggered ones may exceed the critical value, which will lead to an avalanchelike triggering of all sections.

We use an electrothermal model of the evolution of a normal domain [32] and modify it for micronwide superconducting strips [17]. Also, the model is supplemented with the classical Kirchhoff equations to estimate the distribution of currents along the circuit at any given time. We simulate voltage pulses: their magnitude and duration for a different number of triggered sections, as well as the optimal values of the resistors. The following parameters are used for modeling: the width of the superconducting strip $w = 1$ μm, the length of one section of the PNR detector $l = 200$ μm (this corresponds to three turns of the meander with about 63-μm-long strips), the thickness $d = 5$ nm, the sheet resistance $R_s = 600\Omega$, the kinetic inductance per square $L_k = 120$ nH, the critical temperature $T_c = 9$ K, the bath temperature is 2 K.

The results of the simulation are presented in Fig. 7: the waveform transients are presented for one–seven simultaneously triggered sections and serial resistor R_p values of 30 and 35Ω. Our simulation predicts that for $R_p = 35\Omega$ a latching of the detector occurs at simultaneous triggering of six and more sections (two top dashed lines). The inset shows the maximum number of sections that can be operated without latching for a given values of R_p and total number of sections of the detector.

For the correct operation of the PNR detector, the values of the resistors should not be much smaller than the

impedance of the coaxial line (50Ω), otherwise it will reduce the number of sections that are triggered without avalanche switching of the detector. On the other hand, the values of the resistors should not be much higher than the resistance of the normal domain appearing after photon absorption, otherwise the redistribution of currents will be insufficient to recover the superconductivity. For a micronwide strip this value is tens of Ohm by the order of magnitude. As can be seen from the simulation, with a decrease in the resistor and an increase in the number of sections, a parallel PNR detector is able to distinguish a larger number of photons.

Also, the problem with parallel PNR is the impossibility to use all the sections of the detector due to avalanche triggering. As can be seen from the inset of Fig. 7, to distinguish, e.g., 19 photons, it is necessary to make a detector with 35 parallel sections, that is almost twice of the sections involved in detection.

Altogether, in the case of parallel PNR, the increase of the number of sections leads to the reduction of the total kinetic inductance of the detector, which leads to a decrease in the voltage pulse duration thus increasing the speed of the detector. But the reduced kinetic inductance makes the detector more prone to the latching effect when the superconducting state is not restored after photon detection.

APPENDIX B: OPTICAL CAVITY DESIGN AND ABSORPTION

Figure 1(c) shows the simple optical cavity we use: Au mirror (80-nm-thick) and Si_3N_4 (160-nm-thick). The absorption index depending on the wavelength for such a structure is calculated to be 31% for a wavelength of 1064 nm (Fig. 8, blue line). This is consistent with the experimental data shown in Fig. 3 (red curve in the main pane): a saturation plateau of the detection efficiency at high bias current corresponds to 100% of the internal quantum efficiency when each absorbed photon produces a photocount.

On the other hand, if we use just twice a combination of alternating 210-nm-thick Al_2O_3 layer + 100-nm-thick Si it is possible to increase the absorption index up to 87.2% at 1550 nm (Fig. 8, orange line).

Finally, the use of a Bragg mirror instead of a gold one increases the absorption index further up to 94.8% at a wavelength of 1550 nm (Fig. 8, green line).

We also measure detection efficiencies for a set of wavelengths ranging from 828 to 1550 nm for detector 2647-1 no. 6 with 0.5-μm-wide strip (Fig. 9). Maximum values of detection efficiencies measured near critical current follow the absorption of the cavity (blue curve in Fig. 8). On the other hand, at wavelengths above 1-μm internal detection efficiency of superconducting microstrips drops: even if a photon is absorbed by the strip the probability to disrupt the superconducting state is not unity and reduces quickly with the increase of the wavelengths. Thus, detection efficiency at 1550 nm becomes smaller than at 1310 nm in spite of the maximum cavity absorption at 1550 nm.
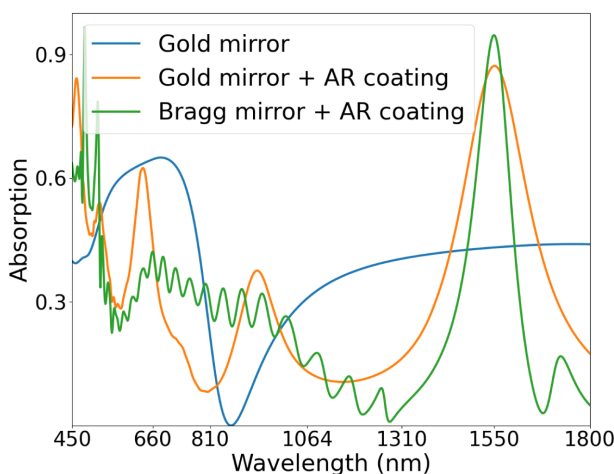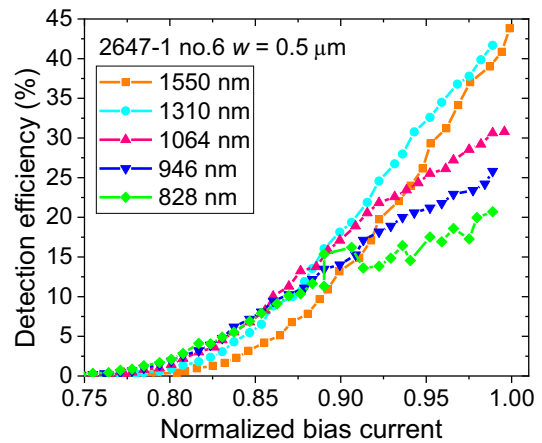

FIG. 9. Detection efficiencies measured for a detector with 0.5-μm-wide strips (2647-1 no. 6). Lower efficiencies at short wavelengths are caused by lower absorption by the cavity (see blue curve in Fig. 8), while smaller efficiency at 1550 nm is caused by a decrease of the internal detection efficiency when not every absorbed photon disrupts superconductivity.

FIG. 8. The theoretically calculated absorbance for the structure used in this paper: gold mirror + Si_3N_4 cavity (blue line), for the same structure but with an AR coating (orange line), and a Bragg mirror + an AR coating (green line).

[1] G. Gol'tsman, O. Okunev, G. Chulkova, A. Lipatov, A. Semenov, K. Smirnov, B. Voronov, A. Dzardanov, G. Williams, and R. Sobolewski, Picosecond superconducting single photon optical detector, Appl. Phys. Lett. **78**, 705 (2001).

[2] A. Engel, J. J. Renema, K. Il'In, and A. Semenov, Detection mechanism of superconducting nanowire single-photon detectors, Supercond. Sci. Technol. **28**, 114003 (2015).

[3] L. You, Superconducting nanowire single-photon detectors for quantum information, Nanophotonics **9**, 2673 (2020).

[4] A. E. Lita, A. J. Miller, and S. W. Nam, Counting near-infrared single-photons with 95% efficiency, Opt. Express **16**, 3032 (2008).

[5] D. V. Reddy, R. R. Nerem, S. W. Nam, R. P. Mirin, and V. B. Verma, Superconducting nanowire single-photon detectors with 98% system detection efficiency at 1550 nm, Optica **7**, 1649 (2020).

[6] F. Mattioli, Z. Zhou, A. Gaggero, R. Gaudio, S. Jahanmirinejad, D. Sahin, F. Marsili, R. Leoni, and A. Fiore, Photon-number-resolving superconducting nanowire detectors, Supercond. Sci. Technol. **28**, 104001 (2015).

[7] A. Divochiy, F. Marsili, D. Bitauld, A. Gaggero, R. Leoni, F. Mattioli, A. Korneev, V. Seleznev, N. Kaurova, O. Minaeva, G. Gol'tsman, K. G. Lagoudakis, M. Benkhaoul, F. Lévy, and A. Fiore, Superconducting nanowire photon-number-resolving detector at telecommunication wavelengths, Nat. Photon. **2**, 302 (2008).

[8] Z. Zhou, S. Jahanmirinejad, F. Mattioli, D. Sahin, G. Frucci, A. Gaggero, R. Leoni, and A. Fiore, Superconducting series nanowire detector counting up to twelve photons, Opt. Express **22**, 3475 (2014).

[9] D. Sahin, A. Gaggero, Z. Zhou, S. Jahanmirinejad, F. Mattioli, R. Leoni, J. Beetz, M. Lermer, M. Kamp, S. Höfling,

and A. Fiore, Waveguide photon-number-resolving detectors for quantum photonic integrated circuits, Appl. Phys. Lett. **103,** 111116 (2013).

[10] M. Moshkova, A. Divochiy, P. Morozov, Y. Vakhtomin, A. Antipov, P. Zolotov, V. Seleznev, M. Ahmetov, and K. Smirnov, High-performance superconducting photon-number-resolving detectors with 86% system efficiency at telecom range, J. Opt. Soc. Am. B **36,** B20 (2019).

[11] C. Cahall, K. L. Nicolich, N. T. Islam, G. P. Lafyatis, A. J. Miller, D. J. Gauthier, and J. Kim, Multi-photon detection using a conventional superconducting nanowire single-photon detector, Optica **4,** 1534 (2017).

[12] D. Zhu, M. Colangelo, C. Chen, B. A. Korzh, F. N. Wong, M. D. Shaw, and K. K. Berggren, Resolving photon numbers using a superconducting nanowire with impedance-matching taper, Nano Lett. **20,** 3858 (2020).

[13] M. Colangelo, *et al.*, Impedance-matched differential superconducting nanowire detectors, (2021), ArXiv:2108.07962.

[14] M. Endo, T. Sonoyama, M. Matsuyama, F. Okamoto, S. Miki, M. Yabuno, F. China, H. Terai, and A. Furusawa, Quantum detector tomography of a superconducting nanostrip photon-number-resolving detector, Opt. Express **29,** 11728 (2021).

[15] F. Mattioli, Z. Zhou, A. Gaggero, R. Gaudio, R. Leoni, and A. Fiore, Photon-counting and analog operation of a 24-pixel photon number resolving detector based on superconducting nanowires, Opt. Express **24,** 9067 (2016).

[16] Y. P. Korneeva, D. Y. Vodolazov, A. V. Semenov, I. N. Florya, N. Simonov, E. Baeva, A. A. Korneev, G. N. Goltsman, and T. M. Klapwijk, Optical Single-Photon Detection in Micrometer-Scale NbN Bridges, Phys. Rev. Appl. **9,** 064037 (2018).

[17] M. Dryazgov, A. Semenov, N. Manova, Y. Korneeva, and A. Korneev, Modelling of normal domain evolution after single-photon absorption of a superconducting strip of micron width, J. Phys.: Conf. Ser. **1695,** 012195 (2020).

[18] Y. P. Korneeva, N. N. Manova, M. A. Dryazgov, N. O. Simonov, P. I. Zolotov, and A. A. Korneev, Influence of sheet resistance and strip width on the detection efficiency saturation in micron-wide superconducting strips and large-area meanders, Supercond. Sci. Technol. **34,** 084001 (2021).

[19] P. I. Zolotov, A. V. Semenov, A. V. Divochiy, G. N. Goltsman, N. R. Romanov, and T. M. Klapwijk, Dependence of photon detection efficiency on normal-state sheet resistance in marginally superconducting films of NbN, IEEE Trans. Appl. Supercond. **31,** 1 (2021).

[20] J. R. Clem and K. K. Berggren, Geometry-dependent critical currents in superconducting nanocircuits, Phys. Rev. B **84,** 174510 (2011).

[21] J. R. Clem and V. G. Kogan, Kinetic impedance and depairing in thin and narrow superconducting films, Phys. Rev. B **86,** 174521 (2012).

[22] D. Y. Vodolazov, Single-Photon Detection by a Dirty Current-Carrying Superconducting Strip Based on the Kinetic-Equation Approach, Phys. Rev. Appl. **7,** 034014 (2017).

[23] M. Dryazgov, N. Simonov, Y. Korneeva, and A. Korneev, Determination of measurement fidelity for a superconducting photon-number resolving detector with micron-wide strips, J. Phys.: Conf. Ser. **2086,** 012177 (2021).

[24] L. A. Morais, T. Weinhold, M. P. de Almeida, A. Lita, T. Gerrits, S. W. Nam, A. G. White, and G. Gillett, Precisely determining photon-number in real-time (2020), ArXiv:2012.10158v2.

[25] J. Chang, J. W. N. Los, J. O. Tenorio-Pearl, N. Noordzij, R. Gourgues, A. Guardiani, J. R. Zichi, S. F. Pereira, H. P. Urbach, V. Zwiller, S. N. Dorenbos, and I. E. Zadeh, Detecting telecom single photons with ($99.5^{+0.5}_{-2.07}$ system detection efficiency and high time resolution, APL Photon. **6,** 036114 (2021).

[26] R. Cheng, Y. Zhou, S. Wang, M. Shen, T. Taher, and H. X. Tang, A 100-pixel photon-number-resolving detector unveiling photon statistics, Nat. Photon. **17,** 112 (2023).

[27] Y. Zhai, F. E. Becerra, B. L. Glebov, J. Wen, A. E. Lita, B. Calkins, T. Gerrits, J. Fan, S. W. Nam, and A. Migdall, Photon-number-resolved detection of photon-subtracted thermal light, Opt. Lett. **38,** 2171 (2013).

[28] J. L. Habif, A. Jagannathan, S. Gartenstein, P. Amory, and S. Guha, Quantum-limited discrimination of laser light and thermal light, Opt. Express **29,** 7418 (2021).

[29] M. Cattaneo, M. G. A. Paris, and S. Olivares, Hybrid quantum key distribution using coherent states and photon-number-resolving detectors, Phys. Rev. A **98,** 012333 (2018).

[30] J. M. Arrazola, *et al.*, Quantum circuits with many photons on a programmable nanophotonic chip, Nature 591, 54 (2021). ArXiv:2103.02109,.

[31] O. S. Magaña-Loaiza, R. d. J. León-Montiel, A. Perez-Leija, A. B. U'Ren, C. You, K. Busch, A. E. Lita, S. W. Nam, R. P. Mirin, and T. Gerrits, Multiphoton quantum-state engineering using conditional measurements, npj Quantum Inf. 5, 80 (2019). ArXiv:1901.00122,.

[32] J. Yang, A. Kerman, E. Dauler, V. Anant, K. Rosfjord, and K. Berggren, Modeling the electrical and thermal response of superconducting nanowire single-photon detectors, IEEE Trans. Appl. Supercond. **17,** 581 (2007).